

(Supplementary information)

Study of the interplay between N-graphene defects and small Pd clusters for enhanced hydrogen storage via the spillover mechanism

E. Rangel,^{‡a} E. Sansores,^b E. Vallejo,^a A. Hernández-Hernández,^a and P. A. López-Pérez^a

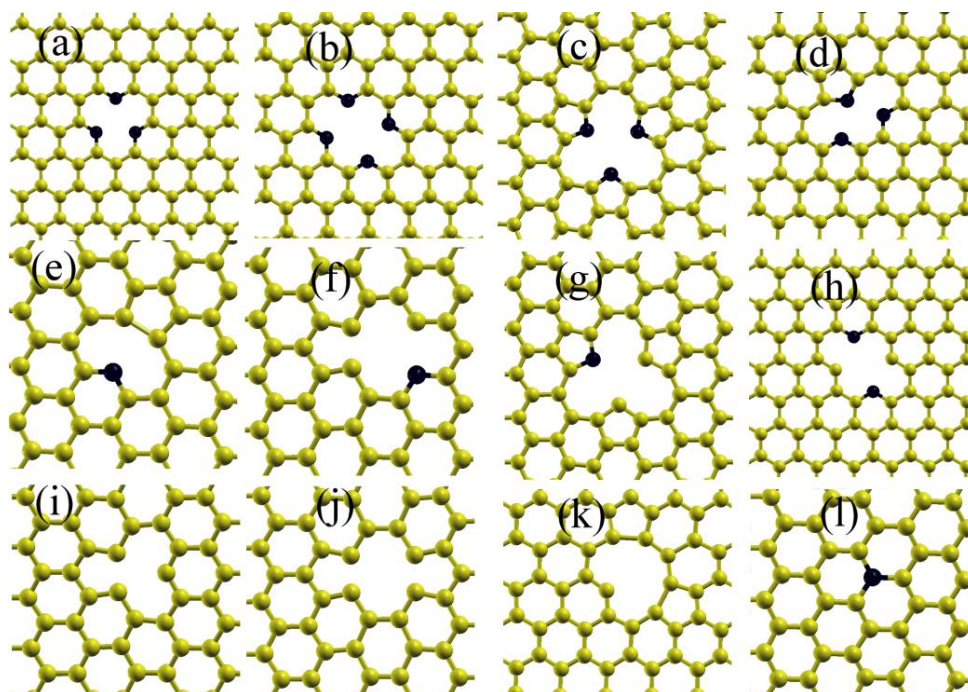


Figure S1. Optimized stable structures of different substrates: in (a) N_3V_1 pyridinic defect, (b) N_4V_2 pyridinic defect, (c) N_3V_3 pyrrolic defect (d), N_3V_1 pyrrolic defect (e) N_1V_1 pyridinic defect, (f) N_1V_2 pyridinic defect, (g) N_1V_3 pyrrolic defect, (h) N_2V_2 pyridinic defect, (i), (j) and (k) V_1, V_2 and V_3 , respectively, and (l) graphitic defect.

^aEscuela Superior de Apan, Universidad Autónoma del Estado de Hidalgo. Carretera Apan-Calpulalpan Km. 8, Col. Chimalpa, C.P. 43920, Apan, Hidalgo, México

^bInstituto de Investigaciones en Materiales, Universidad Nacional Autónoma de México, Apartado Postal 70-360, C.P. 04510, México, D. F., México

Electronic Supplementary Information (ESI)

‡Corresponding author email: kovoldedu@yahoo.com.mx

Table S1. Formation energies (pyrrolic and pyridinic defects) ΔE_f (eV), magnetic moment $m(\mu_B)$, total charge of nitrogen Q_N (e) and C-N bond length \AA .

System	ΔE_f	m	Q_N	C-N
N_3V_1 -pyridinic 49 (31 atoms)	3.30	0.35(0.37)	-0.19(-0.19)	1.33(1.35)
N_2V_1 -pyridinic	4.60	0.52	-0.21	1.34
N_1V_1 -pyridinic	5.14	0	-0.27	1.32
V_1	7.29	1.10	-	-
N_4V_2 -pyridinic	3.65	0.00	-0.18	1.33
N_3V_2 -pyridinic	5.24	0.88	-0.20	1.33
N_2V_2 -pyridinic	6.86	1.90	-0.20	1.34
N_1V_2 -pyridinic	7.18	0.82	-0.18	1.34
V_2	7.05	0.00	-	-
N_3V_3 -pyrrolic	8.07	0.10	-0.22	1.38
N_2V_3 -pyrrolic	9.65	1.38	-0.26	1.39
N_1V_3 -pyrrolic	11.46	2.71	-0.27	1.40
V_3	10.08	1.01	-	-
N_3V_1 -pyrrolic	5.52	0.92	-0.15	1.35
N_1V_1 -pyrrolic	5.14	0.00	-0.27	1.32

1. Simulation details and transferability for the pseudopotentials

For our systems, non-relativistic spin polarized calculations were performed. The cut-off energy was set at 1360 eV and a total of 68 k points within the Monkhorst-Pack special k point scheme⁵¹ were used. The threshold energy convergence was set at 10^{-6} eV and the structural parameters were fully optimized within a force convergence criterion of 0.01 eV/ \AA .

Periodic boundary conditions within an hexagonal unit cell, for pyridinic ($a = b = 9.75 \text{ \AA}$; $c = 30 \text{ \AA}$, see Figure 1, and $a = b = 12.20 \text{ \AA}$; $c = 30 \text{ \AA}$) and pyrrolic ($a = b = 12.20 \text{ \AA}$; $c = 30 \text{ \AA}$) models were chosen. The magnitude of c for both systems was large enough to avoid non-desired interactions between adjacent layers along this direction.

Electronic valence states considered in this work were: hydrogen 1s, carbon $2s^2 2p^2$, oxygen $2s^2 2p^4$, palladium $4d^9 5s^1$, and nitrogen $2s^2 2p^3$. Pseudopotentials and methodologies were validated performing the following calculations. By energy minimization, the length of hydrogen molecule bond was calculated. With PBE functional, it was obtained 0.751 \AA in agreement⁵² with the corresponding experimental value 0.742 \AA . In the same way for palladium, a lattice parameter (FCC, face cubic centered) of 3.98 \AA (3.932 \AA with HSE) and a cohesive energy of 3.90 eV (3.885 eV with HSE) were calculated (the experimental values⁵³ are 3.89 \AA and 3.89 eV respectively). Using the same approach, we obtained for carbon bond-length in graphene 1.419 \AA , (1.411 \AA for HSE) (experimental value is 1.415 \AA). In this way, the error for lattice parameter is reduced from 2.31% (PBE) to 1.079% (HSE). In the same way, the error for cohesive energy is reduced from 0.257% (PBE) to 0.128% (HSE). Thus, the results obtained with HSE exhibit significantly smaller errors

than GGA-PBE. However, both functionals predict with good approximation the structural properties of Palladium (FCC, face cubic centered).

2. Electronic structure and magnetic properties

The red surface with positive is the concentrated electronic charge region. The blue one, with negative, is the region where the electronic charge was lost after the interaction between the atom and the N-graphene surface. In this way, Figure S2 shows transference of extended charge (first and second neighbor carbon atoms, red surface) for Pd- N_3V_3 pyrrolic defect. This effect did not occur for Pd- N_3V_1 pyridinic defect. Projected and total Density of States (PDOS and DOS, respectively) of N_3V_1 pyridinic and N_3V_3 pyrrolic defects with and

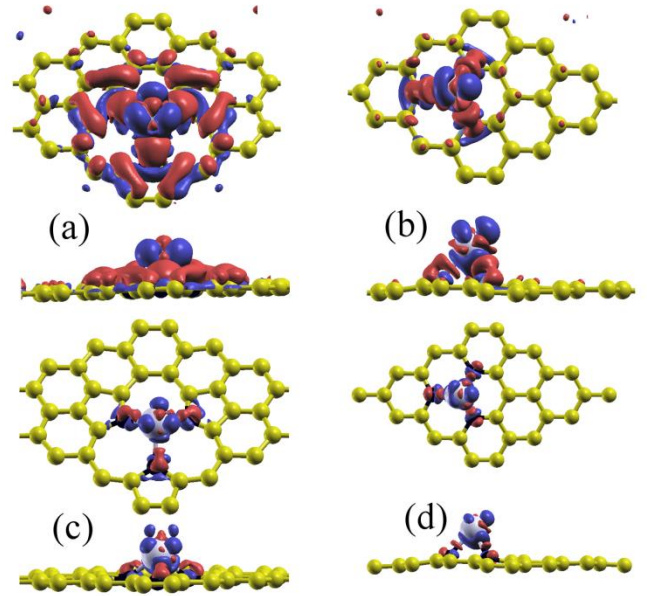


Figure S2. Two surfaces (positive and negative) of constant electron-density difference ($\Delta\rho$) for N_3V_3 pyrrolic defect (left) and N_3V_1 pyridinic defect (right). The red surface with positive $\Delta\rho$ is the concentrated electronic charge region. The blue one, with negative $\Delta\rho$, is the region where the electronic charge was lost after the interaction between the atom and the N-graphene surface. The isosurfaces of constant electron-density difference plotted correspond to values of $\Delta\rho(r) = \pm 1.00 \times 10^{-3} e/a.u.^3$ for (a) Pd on N_3V_3 pyrrolic defect, (b) Pd on N_3V_1 pyridinic defect. (c) and (d) $\Delta\rho(r) = \pm 7.00 \times 10^{-2} e/a.u.^3$ for Pd on N_3V_3 pyrrolic defect and Pd on N_3V_1 pyridinic defect, respectively)

without Pd can be observed in Figure S3. Dirac's point that is presented in pristine graphene is pushed away above Fermi's energy in the case of N_3V_1 pyridinic defect without Pd. When Pd atom is introduced, covering of states of Pd and p-states of C and N are placed inside a Dirac's point-like very near to the Fermi's energy. In the same way, the breakdown of spin symmetry and the appearance of magnetism are found. On the

other hand, d-orbitals (d_{zx} , d_{zy} , $d_{x^2-y^2}$ and d_{xy}) contribution of Pd are presented at the Fermi's energy and the Dirac's point is pushed away above this energy in N_3V_3 pyrrolic defect. Besides, a general covering between d-orbitals of Pd and p-orbitals of Carbon and Nitrogen atoms is observed and a total contribution of hybridized π carbon orbitals are shown to compare with DOS in the case of both N_xV_y defects.

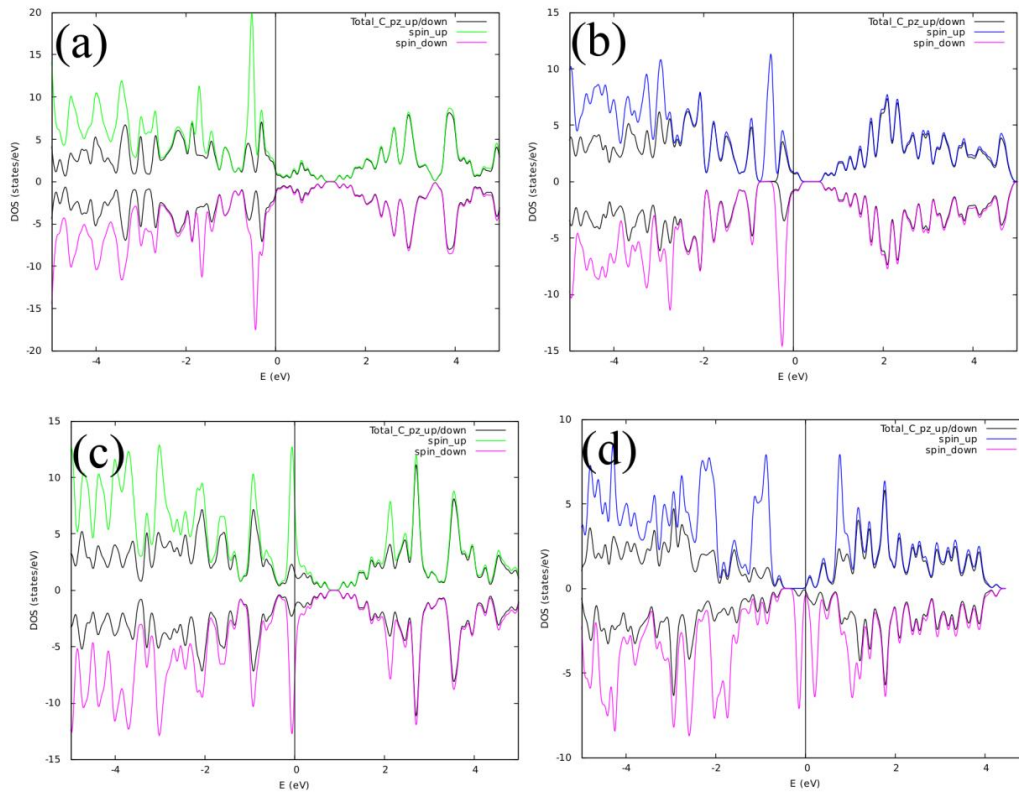


Figure S3. Projected and total density of states (DOS) are shown as a function of energy in eV. In (a) and (c) DOS of N_3V_3 defects without and with Pd contribution respectively are presented. In the same way (b) and (d) represent DOS of N_3V_1 defects without and with Pd contribution. Fermi energy is located at 0 eV.

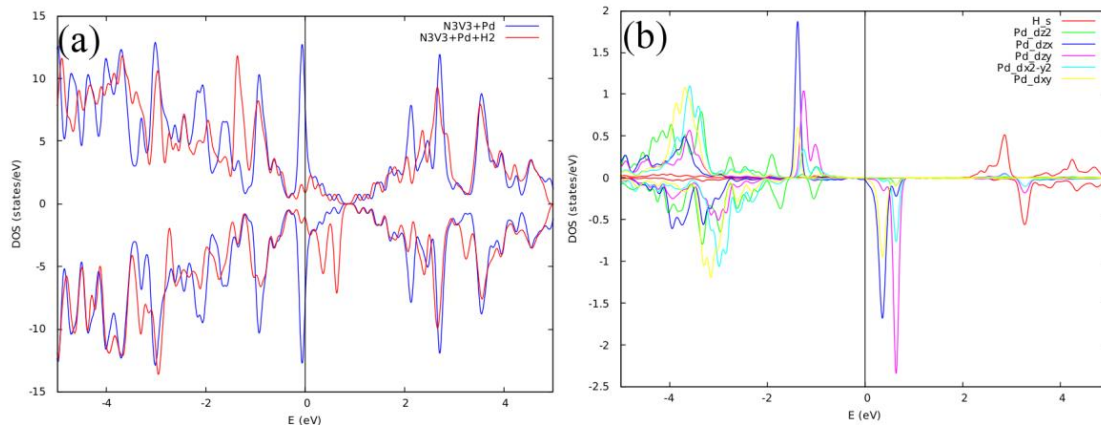


Figure S4: This figure represents the $N_3V_3+Pd+H_2$ system. In (a) Density of States (DOS) vs E (eV) with and without hydrogen can be observed. In (b) Projected Density of States (PDOS) vs E (eV) for d-Pd and s-H orbitals. Fermi energy at 0.

Table S2. Local magnetic moments are presented in accord to Figures S5 (a), (b), (c) and (d).

Atom	N_3V_3 Polarization	$N_3V_3+Pd_1$ Polarization	$N_3V_3+Pd_2$ Polarization	$N_3V_3+Pd_3$ Polarization	$N_3V_3+Pd_4$ Polarization
N1	+0.0310	-0.0000	+0.1319	+0.0770	+0.0238
N2	+0.0316	-0.0003	+0.2134	+0.0759	+0.0230
N3	+0.0312	+0.0002	+0.1652	+0.1950	+0.0225
C1	-0.0025	+0.0000	-0.0093	-0.0015	+0.0020
C2	-0.0025	-0.0000	-0.0017	-0.0011	+0.0018
C3	-0.0025	+0.0000	-0.0051	-0.0008	+0.0020
C4	-0.0025	+0.0000	-0.0047	-0.0012	+0.0021
C5	-0.0024	-0.0000	+0.0131	-0.0001	+0.0015
C6	-0.0024	-0.0000	-0.0048	-0.0002	+0.0016
Pd1	-	-0.0002	+1.1264	+0.9204	+0.3354
Pd2	-	-	+0.1082	+0.7427	+0.5814
Pd3	-	-	-	+0.7428	+0.5828
Pd4	-	-	-	-	+0.5731

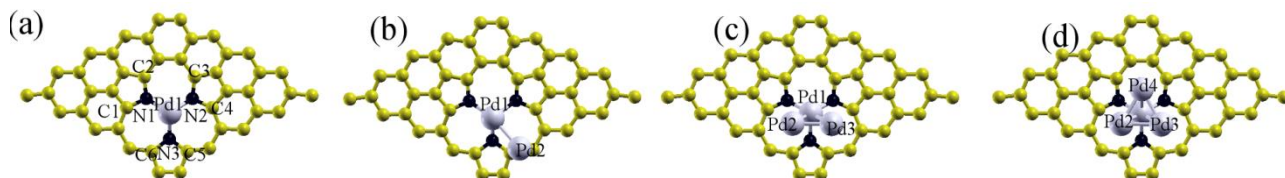


Figure S5. Pd atom and Pd₂, Pd₃ and Pd₄ clusters supported on N_3V_3 -pyrrolic defect.

Local magnetic moments can be observed in Table S2 in accord to Figure S5. In Pd and N atoms, a general one-direction alignment was obtained (a ferromagnetic-like behaviour). Besides for the case of one Pd-atom no magnetic behaviour was calculated. A magnetic moment distribution where a local magnetic moment value reduction was obtained each time the Pd (from Pd2 to Pd4) cluster size increases

Table S3. Complexes adsorption energies $E_{ad_{Pd_m}pH}$ (eV) and barrier energy for migration with PBE (GGA) and HSE hybrid functional

System	Complex adsorption Energy (PBE)	Complex adsorption energy (HSE)	Barrier energy for H migration (HSE)	(PBE)
pyridinic-Pd ₃ -2H	2.98	3.1	2.25	2.09
pyrrolic-Pd ₃ -2H	4.12	4.25	1.75	1.59
pyrrolic-Pd ₄ -2H	4.21	4.38	2.22	1.99
pyridinic-Pd ₄ -2H	3.88	4.02	1.79	1.64
Pyridinic-Pd ₄ -4H	3.9	4.12	0.98	0.84
Pyrrolic-Pd ₄ -4H	4.2	4.35	1.5	1.34
pyrrolic-Pd ₄ H ₂ -6H	4.16	4.28	0.63	0.5

3. Hydrogen storage for different systems at 25 °C temperature and at two different pressures

The results of a systematic study of hydrogen storage on graphene, graphene with palladium, nitrogen-doped graphene and nitrogen-doped

graphene with palladium were reported by Vinayan Bhagavathi.^{S4}

In the following table (Table S4) we show the weight percentage (wt%) of hydrogen storage for different systems at 25 °C temperature and at two

different pressures 2 Mpa and 4 Mpa.^{S4}

Comparing the hydrogen uptake capacity at 25 °C and at 2 MPa, it is observed that the uptake capacity increases from 0.53% for graphene to 0.60% for graphene-palladium. Even so at 4MP the uptake capacity increases from 0.70% to 0.81% (see table S4). It means that there is an increase of hydrogen about 0.07% and 0.11% for 2MP and 4MP respectively. This could be attributed to the presence of micro-pores in the graphene sheets and also indicates the inefficient hydrogen adsorption by the Pd particle agglomerates (sized of 50 nm). These results suggest that the migration of hydrogen via spillover is thermodynamically and kinetically very difficult and would not happen in normal conditions.

However for the N-graphene-Pd and N-graphene systems, the uptake capacity increases from 0.88% to 1.97 % (difference of 1.09%) at 2MP, and also from 1.47% to 4.40 % at 4MP (difference of 2.93%), see Table S4.

Table S4. The weight percentage (wt%) of hydrogen storage for different systems at 25 °C temperature and at two different pressures

System	wt % at 2MP	wt % at 4MP
graphene	0.53	0.70
graphene-palladium	0.60	0.81
nitrogen-graphene	0.88	1.47
nitrogen-graphene-palladium	1.97	4.40

The former results suggest that the interaction between the hydrogen gas and the nitrogen-doped graphene with Palladium is stronger than the pristine graphene with Palladium.

As consequence we suggest that the nitrogen-graphene support plays two important roles:

1. The nitrogen atoms effectively change the chemical properties of the support resulting in transfer of electrons from the Pd atom to support and in high dispersion and electron deficiency in Pd particles.

2. The highly dispersed and strongly adhered Pd nanoparticles and small clusters decrease the

dissociation/migration barriers of hydrogen molecules/atoms at room temperature.

References

S1 H. J. Monkhorst and J. D. Pack, *Phys. Rev. B*, 1976, **13**, 5188-5192

S2 *Handbook of chemistry and physics*, ed. D. R. Lide, CRC Press LLC, Boca Raton, 76th Edition, 2000.

S3 C. Kittel, *Introduction to solid state physics*, Wiley, New York, 8th Edition, 2005.

S4. V. B. Parambath, R. Nagar and S. Ramaprabhu, *Langmuir*, 2012, **28**, 7826-7833.